A Spin Cell for Spin Current

Qing-feng Sun,[1,2] Hong Guo,[1,2] and Jian Wang[3]
[1]Center for the Physics of Materials and Department of Physics, McGill University, Montreal, PQ, Canada H3A 2T8
[2]Institute of Physics, Chinese Academy of Sciences, Beijing 100080, China
[3]Department of Physics, The University of Hong Kong, Pokfulam Rood, Hong Kong, China
(Received 12 December 2002; published 26 June 2003)

We propose and investigate a spin-cell device which provides the necessary spin-motive force to drive a spin current for future spintronic circuits. Our spin cell has four basic characteristics: (i) it has two poles so that a spin current flows in from one pole and out from the other pole, and in this way a complete spin circuit can be established; (ii) it has a source of energy to drive the spin current; (iii) it maintains spin coherence so that a sizable spin current can be delivered; (iv) it drives a spin current without a charge current. The proposed spin cell for spin current should be realizable using technologies presently available.

DOI: 10.1103/PhysRevLett.90.258301 PACS numbers: 85.35.–p, 73.23.–b, 72.25.Pn, 73.40.Gk

Traditional electronics is based on the flow of charge: the spin of the electron is ignored. The emerging technology of spintronics will make the leap such that the flow of spin, in addition to charge, will be used for electronic applications [1,2]. A spin current is produced by the motion of spin-polarized electrons; therefore spin current is typically associated with the spin-polarized charge current [1]. Nevertheless, if one can generate an ideal situation, as shown in Fig. 1(a), where spin-up electrons move to the right while an equal number of spin-down electrons move to the left, then there will be no net charge current because $I_e \equiv e(I_\uparrow + I_\downarrow) = 0$, where $eI_\uparrow, eI_\downarrow$ are charge currents due to spin-up and spin-down electrons, respectively. There will be, however, a finite spin current: $I_s \equiv \frac{\hbar}{2}(I_\uparrow - I_\downarrow)$ where $\hbar$ is the reduced Planck constant. Considering the interesting and important future perspective of spin-current circuits, it is crucial to have a spin cell that satisfies the four characteristics discussed in the abstract and it produces the flow pattern of Fig. 1(a) [3]. In this paper we theoretically propose and analyze such a spin cell.

Our spin cell is schematically shown in Fig. 1(b). It consists of a double quantum dot (QD) fabricated in two-dimensional electron gas (2DEG) with split gate technology, and each QD is contacted by an electrode. Note that no magnetic material is involved. The two QDs and their associated contacts to the electrodes serve as the "positive" or "negative" poles of the spin cell. The two electrodes maintain the same electrochemical potential $\mu_L = \mu_R$ (i.e., no bias voltage is applied on them). The size of the spin-cell structure is assumed to be within the spin-coherence length which can be as long as many microns for 2DEG. We control the QD energy levels by gate voltages $V_{g\alpha}$ where $\alpha = L, R$ indicates the left/right QD. Both QD levels are controlled by an overall gate voltage V_g; see gate arrangements in Fig. 1(b). In order to distinguish spin-up electrons from spin-down electrons, a spatially *nonuniform* external magnetic field B_α is applied to the two QDs—perpendicular to the QD plane. An extreme case of nonuniformity is $B_R = -B_L$, i.e., equal in value but opposite in direction. This particular magnetic field distribution is not necessary at all for the operation of our spin cell, but it helps us to discuss its physics. Finally, the energy source of our spin cell is provided by shining a microwave radiation with strengths Δ_L/Δ_R for the left/right QDs. Because, typically, the microwave frequency is far less than the plasma frequency of the material covering the QDs, the effect of the microwave field is to induce a high frequency potential variation $\Delta_{L/R}\cos\omega t$ in the left/right QD and their leads [4]. When $\Delta_L \neq \Delta_R$, a time-dependent potential difference, $\Delta\cos\omega t = (\Delta_L - \Delta_R)\cos\omega t$, exists between the two QDs. An ac electric field $\mathbf{E}(t)$ in the middle barrier is therefore established due to microwave radiation [see Fig. 1(c)]. Then, electrons can absorb photons when they pass the middle barrier of the device. The establishment of $\mathbf{E}(t)$ across the two QDs is necessary

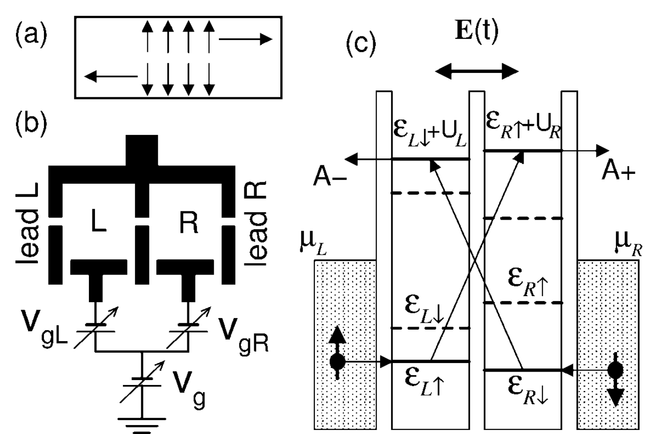

FIG. 1. (a) Schematic diagram for a conductor which has a spin current with zero charge current; (b) schematic diagram for the double quantum dot spin cell; (c) schematic plot for the spin-cell operation via photon assisted tunneling processes indicated by $A\pm$.

for our spin cell to work; here, we use a nonuniform microwave radiation to achieve this effect as has already been carried out experimentally [5], but other possibilities also exist.

Before we present theoretical and numerical results of the device in Fig. 1(b), we first discuss why it works as a spin cell. The physics is summarized in Fig. 1(c). To be specific, let B_R point to the $-z$ direction and B_L to the $+z$ direction. Because of the Zeeman effect, a spin-degenerate level ϵ_R on the right QD is now split into spin-down/spin-up levels $\epsilon_{R\downarrow} < \epsilon_{R\uparrow}$. On the left QD, it is $\epsilon_{L\uparrow} < \epsilon_{L\downarrow}$. Electrons in the electrodes can now tunnel into the QD: on the right a spin-down electron is easier to tunnel because level $\epsilon_{R\downarrow}$ is lower, while a spin-up electron is easier to tunnel into the left QD. Once levels $\epsilon_{R\downarrow}$, $\epsilon_{L\uparrow}$ are occupied, the charging energies U_R, U_L of the two QDs push the other two levels $\epsilon_{R\uparrow}$, $\epsilon_{L\downarrow}$ to higher energies $\epsilon_{R\uparrow} + U_R$, $\epsilon_{L\downarrow} + U_L$, and the energy level positions indicated by the solid horizontal lines of Fig. 1(c) are established. Next, the spin-down electron on the right QD can absorb a photon and make a transition to the level at $\epsilon_{L\downarrow} + U_L$ on the left QD: afterwards it easily flows out to the left electrode because $\epsilon_{L\downarrow} + U_L > \mu_L$. This process is indicated as $A-$. Similarly the spin-up electron on the left QD flows out to the right electrode after absorption of a photon, indicated by $A+$. This way, driven by the potential variations of the QD induced by the microwave field, a spin-down electron flows to the left while a spin-up electron flows to the right of the spin cell, and the continuation of the $A-$, $A+$ processes generates a dc spin current that flows from the left electrode, through the spin cell, and out to the right electrode. Clearly, if the two processes are absolutely equivalent, there will be no charge current and only a spin current. Finally, since the spin-motive force is provided by a time-dependent change of the electronic potential landscape of the QD, there is no spin-flip mechanism and the spin current flowing through the spin cell is conserved, i.e., $I_{s,L} = -I_{s,R} = I_s$. Our device then satisfies the four characteristics of a spin cell discussed in the abstract.

The last paragraph discusses the operation principle of the spin cell for spin current, but there are other interesting device details which can be obtained only by detailed theoretical and numerical analysis for which we now turn. The spin cell of Fig. 1(b) is described by the following Hamiltonian [4,6]:

$$
\begin{aligned}
H = &\sum_{\alpha\sigma}[\epsilon_\alpha + W_\alpha(t) - (1/2)\sigma g\mu B_\alpha]d^\dagger_{\alpha\sigma}d_{\alpha\sigma} \\
&+ \sum_\alpha U_\alpha d^\dagger_{\alpha\uparrow}d_{\alpha\uparrow}d^\dagger_{\alpha\downarrow}d_{\alpha\downarrow} + \sum_{k\sigma\alpha}[\epsilon_{\alpha k} + W_\alpha(t)]a^\dagger_{\alpha k\sigma}a_{\alpha k\sigma} \\
&+ \sum_{k\sigma\alpha}[t_{\alpha k}a^\dagger_{\alpha k\sigma}d_{\alpha\sigma} + \text{H.c.}] + \sum_\sigma[t_C d^\dagger_{L\sigma}d_{R\sigma} + \text{H.c.}],
\end{aligned}
\tag{1}
$$

where $a^\dagger_{\alpha k\sigma}$ ($a_{\alpha k\sigma}$) and $d^\dagger_{\alpha\sigma}$ ($d_{\alpha\sigma}$) are creation (annihilation) operators in the electrode α and the dot α, respectively. The left and right QDs include a single energy level ϵ_α that has spin index σ and intradot Coulomb interaction U_α. To account for the magnetic field B, the left/right QD's single particle energy has a term $-(1/2)\sigma g\mu B_\alpha$, in which we have required a different magnetic field strength for the two QDs, i.e., $B_L \neq B_R$. t_C and $\Gamma_\alpha \equiv 2\pi\sum_k|t_{\alpha k}|^2\delta(\epsilon - \epsilon_{\alpha k})$ describe the coupling strength between the two QDs, and between electrode α and its corresponding QD, respectively. The microwave irradiation is given by $W_\alpha(t) = \Delta_\alpha\cos\omega t$ [4,6] and it produces an adiabatic change for the single particle energy. Here we permit the microwave field to irradiate the entire device including the electrodes, and we require a difference in the radiation strength $\Delta_L \neq \Delta_R$.

Our theoretical analysis of the spin cell is based on standard Keldysh nonequilibrium Green's function theory [4,6] which we briefly outline here. First, we perform a unitary transformation of the Hamiltonian with a unitary operator $U(t) = \exp\{i\int_0^t dt'\sum_\alpha W_\alpha(t')\hat{D}_\alpha\}$, where $\hat{D}_\alpha \equiv \sum_{k\sigma}a^\dagger_{\alpha k\sigma}a_{\alpha k\sigma} + \sum_\sigma d^\dagger_{\alpha\sigma}d_{\alpha\sigma}$. The Hamiltonian H is transformed to the following form:

$$
\begin{aligned}
H = &\sum_{\alpha\sigma}[\epsilon_\alpha - \sigma g\mu B_\alpha/2]d^\dagger_{\alpha\sigma}d_{\alpha\sigma} + \sum_\alpha U_\alpha d^\dagger_{\alpha\uparrow}d_{\alpha\uparrow}d^\dagger_{\alpha\downarrow}d_{\alpha\downarrow} \\
&+ \sum_{k\sigma\alpha}\epsilon_{\alpha k}a^\dagger_{\alpha k\sigma}a_{\alpha k\sigma} + \sum_{k\sigma\alpha}[t_{\alpha k}a^\dagger_{\alpha k\sigma}d_{\alpha\sigma} + \text{H.c.}] \\
&+ \sum_\sigma[t_C e^{i\int_0^t dt'\Delta\cos\omega t'}d^\dagger_{L\sigma}d_{R\sigma} + \text{H.c.}],
\end{aligned}
\tag{2}
$$

where $\Delta \equiv \Delta_L - \Delta_R$. In (2), we take the last term which explicitly depends on time t as the interacting part H_I and the remaining part as $H_0 \equiv H - H_I$. The Green's function of H_0, $g^r(\epsilon)$, can be easily obtained with a decoupling approximation at the Hartree level [7]:

$$
g^r_{\alpha\alpha\sigma}(\epsilon) = \frac{\epsilon^-_{\alpha\sigma} + U_\alpha n_{\alpha\bar{\sigma}}}{(\epsilon - \epsilon_{\alpha\sigma})\epsilon^-_{\alpha\sigma} + \frac{i}{2}\Gamma_\alpha(\epsilon^-_{\alpha\sigma} + U_\alpha n_{\alpha\bar{\sigma}})}, \tag{3}
$$

where $\epsilon^-_{\alpha\sigma} \equiv \epsilon - \epsilon_{\alpha\sigma} - U_\alpha$, $\epsilon_{\alpha\sigma} \equiv \epsilon_\alpha - \sigma g\mu B_\alpha/2$, and $n_{\alpha\bar{\sigma}}$ is the time-averaged intradot electron occupation number at the state $\bar{\sigma}$ in the α QD which we solve self-consistently. It is worth mentioning that $g^r_{\alpha\alpha\sigma}(\epsilon)$ in Eq. (3) has two resonances: one is at $\epsilon_{\alpha\sigma}$, while its associated state at $\epsilon_{\alpha\bar{\sigma}}$ is empty; the other resonance is at $\epsilon_{\alpha\sigma} + U_\alpha$, while its associated state $\epsilon_{\alpha\bar{\sigma}}$ is occupied. Notice, in H_0 the left part of the spin cell (i.e., the left lead and the left QD) is not coupled with the right part of the spin cell, therefore they are in equilibrium respectively. Hence the Keldysh Green's function $g^<_{\alpha\alpha\sigma}(\epsilon)$ for H_0 can be solved from the fluctuation-dissipation theorem: $g^<_{\alpha\alpha\sigma}(\epsilon) = -f_\alpha[g^r_{\alpha\alpha\sigma}(\epsilon) - g^a_{\alpha\alpha\sigma}(\epsilon)]$. With these preparations, the Green's function G^r and $G^<$ of the total Hamiltonian H can be solved. In particular, we calculate $G^r_{\alpha\beta\sigma}(t,t') \equiv -i\theta(t-t')\langle\{d_{\alpha\sigma}(t), d^\dagger_{\beta\sigma}(t')\}\rangle$ by iterating the Dyson equation. In Fourier space, the Dyson equation can be reduced to [8,9]

$$
\mathbf{G}^r_{\sigma;mn}(\epsilon) = \mathbf{g}^r_{\sigma;mn}(\epsilon) + \sum_k \mathbf{G}^r_{\sigma;mk}(\epsilon)\mathbf{\Sigma}^r_{\sigma;kn}(\epsilon)\mathbf{g}^r_{\sigma;nn}(\epsilon),
$$

where $\mathbf{G}^r_{\sigma,mn}(\epsilon) \equiv \mathbf{G}^r_{\sigma,n-m}(\epsilon + m\omega)$, and the quantity $G_n(\epsilon)$ is the Fourier expansion of $G(t,t')$ [8]. The retarded self-energy $\mathbf{\Sigma}^r_{\sigma;kn}(\epsilon)$ is the Fourier transform of $\mathbf{\Sigma}^r_{\sigma}(t_1,t_2)$ where $\Sigma^r_{LR\sigma}(t_1,t_2) = \Sigma^{r*}_{RL\sigma}(t_1,t_2) = \delta(t_1 - t_2)t_C \exp[i\int_0^{t_1} dt'\Delta\cos\omega t']$, and $\Sigma^r_{LL\sigma} = \Sigma^r_{RR\sigma} = 0$. We obtain $\Sigma^r_{LR\sigma,mn}(\epsilon) = \Sigma^{r*}_{RL\sigma,nm}(\epsilon) = t_C J_{n-m}(\Delta/\omega)$. The Green's function $\mathbf{g}^r_{\sigma;mn}(\epsilon)$ is $g^r_{\alpha\beta\sigma;mn}(\epsilon) = \delta_{\alpha\beta}\delta_{mn}g^r_{\alpha\alpha\sigma}(\epsilon + m\omega)$. Then $\mathbf{G}^r_{\sigma;mn}(\epsilon)$ can be solved from the above Dyson equation [10]:

$$G^r_{\alpha\alpha\sigma,mn}(\epsilon) = \delta_{mn}/[(g^r_{\alpha\alpha\sigma,mm})^{-1} - A_{\bar{\alpha}\sigma,mm}],$$

$$G^r_{\alpha\bar{\alpha}\sigma,mn}(\epsilon) = G^r_{\alpha\alpha\sigma,mm}(\epsilon)\Sigma^r_{\alpha\bar{\alpha}\sigma,mn}g^r_{\bar{\alpha}\bar{\alpha}\sigma,nn}(\epsilon),$$

where $A_{\alpha\sigma,mm}(\epsilon) \equiv \sum_k |t_C|^2 J^2_{k-m}(\Delta/\omega)g^r_{\alpha\alpha\sigma;kk}(\epsilon)$. Afterwards, the total Keldysh Green's function $G^<_{\alpha\beta\sigma}(t,t') \equiv i\langle d^\dagger_{\beta\sigma}(t')d_{\alpha\sigma}(t)\rangle$ is easily obtained from the Keldysh equation. Finally, we obtain the time-averaged current in lead α from

$$I_{\alpha\sigma} \equiv \langle I_{\alpha\sigma}(t)\rangle = -\mathrm{Im}\int (d\epsilon/2\pi)\Gamma_\alpha(\epsilon)[G^<_{\alpha\alpha\sigma,00}(\epsilon) + 2f_\alpha(\epsilon)G^r_{\alpha\alpha\sigma,00}(\epsilon)], \quad (4)$$

and the self-consistent equation for the intradot occupation number $n_{\alpha\sigma}$: $n_{\alpha\sigma} = -i\int(d\epsilon/2\pi)G^<_{\alpha\alpha\sigma,00}(\epsilon)$.

Figure 2 shows the calculated charge current I_e (in units of e) and the spin current I_s (in units of $\hbar/2$) versus the gate voltage V_{gR} at different microwave frequency ω. I_e shows a positive peak due to the $A+$ process and a negative peak by the $A-$ process [see Fig. 1(c)], but I_s has two positive peaks. As we tune the gate voltage V_{gR}, the right QD level is shifted so that when $\hbar\omega = \epsilon_{L\downarrow} + U_L - \epsilon_{R\downarrow}$, the $A-$ process occurs with high probability leading to a positive peak in I_s and a negative peak in I_e. On the other hand we get positive peaks in both I_e and I_s when $\hbar\omega = \epsilon_{R\uparrow} + U_R - \epsilon_{L\uparrow}$, for the $A+$ process.

The peak positions in I_e, I_s due to the $A\pm$ processes shift linearly with the microwave frequency ω, as shown by the dotted lines in Fig. 2. Eventually, at a special frequency indicated by A, i.e., when $\hbar\omega^* = \epsilon_{R\uparrow} + U_R - \epsilon_{L\uparrow} = \epsilon_{L\downarrow} + U_L - \epsilon_{R\downarrow}$, the two peaks overlap so that the net charge current I_e cancels exactly due to the cancellation of the $A\pm$ processes, at the same time the spin current I_s doubles its value. At this special frequency, the full operation of the spin cell occurs so that a spin current is driven across the spin cell, from the left electrode to the right electrode, without a charge current. If we connect the spin cell to complete an external circuit, a spin current will be driven and will continue to flow across the spin cell into the circuit [11]. On the other hand, if we let the two poles of the spin cell open, although I_s must be zero, a spin-motive force in the two poles of the spin cell will still be induced so that chemical potential $\mu_{\alpha\uparrow} \neq \mu_{\alpha\downarrow}$. For example, in the case of Fig. 1(c), an open circuit will lead to $\mu_{L\uparrow} < \mu_{L\downarrow}$ and $\mu_{R\uparrow} > \mu_{R\downarrow}$.

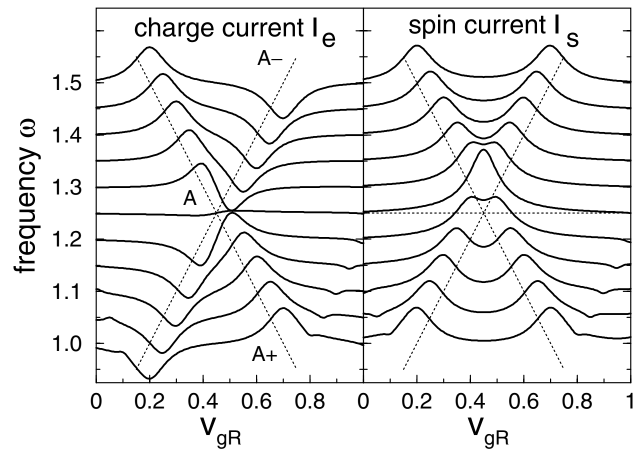

FIG. 2. The charge current I_e and spin current I_s versus gate voltage V_{gR} for different frequencies ω. Different curves have been offset such that the vertical axis gives the frequency. Two dotted oblique lines $A\pm$ indicate the position of the peaks. The parameters are $\mu_L = \mu_R = 0$, $\Gamma_L = \Gamma_R = k_BT = 0.1$, $t_C = 0.02$, $U_L = 1$, $U_R = 0.9$, $g\mu B_L = 0.2$, $g\mu B_R = -0.4$, $V_{gL} = 0.5$, $V_g = 0$, and $\Delta/\omega = 1.0$.

In the following we focus on the spin-cell operation by fixing gate voltage $V_{gR} = 0.45$ which is its value at point A of Fig. 2. We investigate I_e, I_s as functions of the overall gate potential V_g [Fig. 3(a)], magnetic field $g\mu B_L$ [Fig. 3(b)], and frequency ω [Fig. 3(c)]. The different curves in Fig. 3 correspond to different microwave strength $\Delta \equiv \Delta_L - \Delta_R$. In all situations $I_e \approx 0$, and we do not discuss it anymore. Figure 3(c) shows that I_s has several peaks and dips when we vary ω: the large peak indicated by A is the spin-cell operation discussed above, but peaks at C and D correspond to double- and triple-photon processes which connect the $A\pm$ transitions of Fig. 1(c). The dip at B originates from less probable transitions connecting levels indicated by the dashed lines of Fig. 1(c), while the dip at E is its two-photon process. Now, fixing ω at ω^*, i.e., at the spin-cell operation point A, the value of I_s can be tuned by the overall gate voltage V_g as shown in Fig. 3(a). However, I_s keeps large values for a wide range of V_g: this range is in the Coulomb interaction scale U/e. This is important, because in an experimental situation any background charge or environmental effect near the spin cell may alter the overall potential, and Fig. 3(a) shows that the spin-cell operation is not critically altered by this effect. When V_g becomes very large so that $\epsilon_{L\downarrow} + U_L$ and $\epsilon_{R\uparrow} + U_R$ are below the chemical potential μ, or $\epsilon_{L\uparrow}$ and $\epsilon_{R\downarrow}$ are above μ, I_s diminishes because the $A\pm$ processes can no longer occur [see Fig. 1(c)]. Finally, a very important result is shown in Fig. 3(b), where we fixed $g\mu B_R = -0.4$ while varying $g\mu B_L$ at the spin-cell operation point A [12]. Figure 3(b) shows clearly that I_s increases with an increasing difference of $B_L - B_R$: $I_s = 0$ identically when $B_L = B_R$ if $U_L = U_R$, or $I_s \approx 0$ if $U_L \neq U_R$. However, Fig. 3(b) demonstrates that we need only a

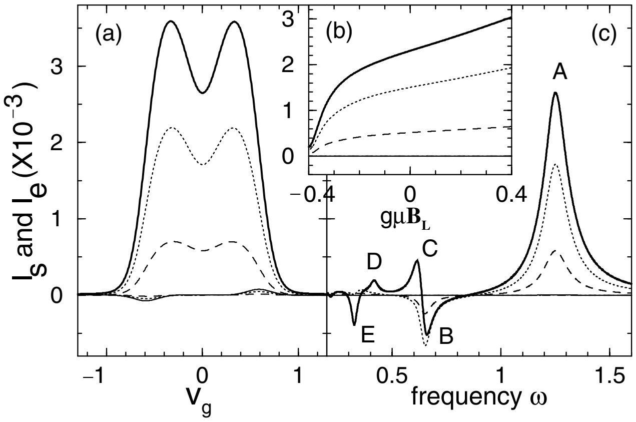

FIG. 3. (a)–(c) are I_e and I_s versus gate voltage V_g, the magnetic field $g\mu B_L$, and frequency ω, respectively. $\omega = 1.25$ in (a); $2\omega = U_L + U_R + g\mu(B_L - B_R)$ in (b). $V_{gR} = 0.45$, and other parameters are the same as Fig. 2. The solid, dotted, and dashed lines correspond to $\Delta/\omega = 2.0, 1.0$, and 0.5, respectively. Notice that the three curves of charge current overlap and they are all essentially zero.

slight difference in B_L and B_R, at a scale of the coupling constant Γ_α, to generate a substantial I_s. The most important fact is that B_L and B_R do not have to point to opposite directions which is experimentally difficult to do. In fact, if the two QDs are fabricated with different materials so that the g factors are different, one can actually use a *uniform* magnetic field throughout.

The proposed spin cell for spin current should be experimentally feasible using present technologies. First, the double-QD structures can and have been fabricated by several laboratories. Second, microwave assisted quantum transport measurements have recently been reported [5,13,14]. In particular, the asymmetrical microwave radiation on the double-QD device (i.e., $\Delta_L \neq \Delta_R$) has already been carried out experimentally [5]. Third, the asymmetric magnetic field should be feasible as we have discussed above. If one takes $f = \omega/2\pi = 50$ GHz, arranges the corresponding $U(\sim\hbar\omega) \approx 0.2$ meV, and fixes the temperature scale K_BT and coupling Γ_α to be 20 times less than U as in typical QD experiments, i.e., $k_BT = 100$ mK and $\Gamma = 10$ μeV, the corresponding magnetic field difference is $[g\mu(B_L - B_R) \sim \Gamma]$ $|B_L - B_R| \sim 0.16/g$ tesla. These QD parameters have already been realized by present technology. Finally, it is not difficult to show that by adjusting the gate voltages one can easily calibrate the spin-cell operating point [15].

We gratefully acknowledge financial support from NSERC of Canada, FCAR of Quebec (Q. S., H. G), the National Science Foundation of China, the Chinese Academy of Sciences (Q. S.), and a RGC grant from the SAR Government of Hong Kong under Grant No. HKU 7091/01P (J.W.). H. G. thanks Dr. Junren Shi for a discussion on photon assisted tunneling. We gratefully acknowledge Dr. Baigeng Wang for many discussions and inputs on the physics of spin current.

[1] S. A. Wolf *et al.*, Science **294**, 1488 (2001).
[2] G. A. Prinz, Science **282**, 1660 (1998).
[3] There has been some work on the spin-current generation by a rotating magnetic field in a unipole device. A unipole system, however, cannot function as a spin cell because it cannot complete a spin circuit. See A. Brataas, Y. Tserkovnyak, G. E.W. Bauer, and B. I. Halperin, Phys. Rev. B **66**, 060404 (2002); B. Wang, J. Wang, and H. Guo, *ibid.* **67**, 092408 (2003).
[4] A.-P. Jauho, N. S. Wingreen, and Y. Meir, Phys. Rev. B **50**, 5528 (1994).
[5] T. H. Oosterkamp *et al.*, Nature (London) **395**, 873 (1998).
[6] N. S. Wingreen, A.-P. Jauho, and Y. Meir, Phys. Rev. B **48**, 8487 (1993).
[7] In deriving the (nonperturbed) retarded Green's function of H_0, we have taken a decoupling approximation as $\langle\langle a_{\alpha k\sigma} d^\dagger_{\alpha\bar\sigma} d_{\alpha\bar\sigma} \mid d^\dagger_{\alpha\sigma}\rangle\rangle^r = n_{\alpha\bar\sigma}\langle\langle a_{\alpha k\sigma} \mid d^\dagger_{\alpha\sigma}\rangle\rangle^r$, $\langle\langle a^\dagger_{\alpha k\bar\sigma} d_{\alpha\sigma} d_{\alpha\bar\sigma} \mid d^\dagger_{\alpha\sigma}\rangle\rangle^r = \langle\langle a_{\alpha k\bar\sigma} d^\dagger_{\alpha\bar\sigma} d_{\alpha\sigma} \mid d^\dagger_{\alpha\sigma}\rangle\rangle^r = 0$. In this approximation the level renormalization has been neglected. Because our system is in the Coulomb blockade regime, the level renormalization is very small and this approximation is reasonable. If the level renormalization is included, it does not affect the working principle of the spin cell.
[8] Q.-f. Sun, J. Wang, and T.-h. Lin, Phys. Rev. B **59**, 13 126 (1999).
[9] Because H_0 has the interaction U_α, this Dyson equation is not exact, but is a good approximation.
[10] Here we took the same approximation as that of Ref. [8] which is justifiable when $\hbar\omega \gg \max(\Gamma_\alpha, t_C)$.
[11] If resistances of external circuits for spin-up and spin-down channels are slightly different, the spin cell will drive a spin current but perhaps with a small charge current. However, by regulating the gate voltage V_g which makes the spin-motive force slightly different for spin-up and spin-down electrons, we can still obtain a spin current with zero charge current.
[12] The frequency ω^* of the spin-cell operation point A [see Fig. 1(c)] actually depends on the value of B_L: $2\hbar\omega^* = \epsilon_{L\downarrow} + U_L + \epsilon_{R\uparrow} + U_R - \epsilon_{L\uparrow} - \epsilon_{R\downarrow} = U_L + U_R + g\mu(B_L - B_R)$. To plot Fig. 3(b) we varied ω^* for each value of B_L accordingly.
[13] T. H. Oosterkamp *et al.*, Phys. Rev. Lett. **78**, 1536 (1997).
[14] L. P. Kouwenhoven *et al.*, Phys. Rev. Lett. **73**, 3443 (1994).
[15] In order to calibrate experimental conditions at the spin-cell operating point, one needs a method to detect spin current outside the spin cell. Recently, Hirsch has advanced a theoretical idea for this purpose which works even in the absence of a charge current: J. E. Hirsch, Phys. Rev. Lett. **83**, 1834 (1999). Moreover, the detection can be made easier if we allow and then detect a small charge current that flows through the spin cell, using the two panels of Fig. 2 as a "map" between the charge and spin currents.